The Characteristics of a 1 m Methanol Pool Fire

Kunhyuk Sung[a], Jian Chen[a], Matthew Bundy,[a] and Anthony Hamins[a*]

[a] National Institute of Standards and Technology, 100 Bureau Dr., Gaithersburg, Maryland, USA

* Tel: +1-301-975-6598, email: anthony.hamins@nist.gov

Highlights:

- The heat release rates determined by calorimetry and mass loss compared favorably
- Temperature profiles in the radial and axial directions were measured
- Gas temperatures were estimated considering radiative loss and thermal inertia effects
- The radiative fraction was calculated as 0.22 ± 16 % from heat flux measurements

Abstract:

A series of measurements was made to characterize the structure of a 1 m diameter methanol (CH_3OH) pool fire steadily burning with a constant lip height in a quiescent environment. Time-averaged local measurements of gas-phase temperature were conducted using 50 µm diameter, Type S, bare wires, with a bead that was approximately spherical with a diameter of about 150 µm. The thermocouple signals were corrected for radiative loss and thermal inertia effects. The mass burning rate was measured by monitoring the mass loss in the methanol reservoir feeding the liquid pool. The heat release rate was measured using oxygen consumption calorimetry. The heat flux was measured in the radial and vertical directions and the radiative fraction was estimated, which corresponded to previous results.

Keywords: Heat release rate; Temperature distribution; Burning rate; Heat flux distribution; Radiative fraction

1. Introduction

The focus of this study is to characterize the burning of a 1 m diameter pool fire steadily burning in a well-ventilated quiescent environment. Pool fires are a fundamental type of combustion phenomena in which the fuel surface is flat and horizontal, which provides a simple and well-defined configuration to test models and further the understanding of fire phenomena. In this study, methanol is selected as the fuel. Fires established by methanol are unusual as no carbonaceous soot is present or emitted. This creates a particularly useful testbed for fire models and their radiation sub models that consider emission by gaseous species - without the confounding effects of radiative exchange due to soot.

Many studies have been reported on the structure and characteristics of 30 cm diameter methanol pool fires, including the total mass loss rate [1-3], mean velocity [4], pulsation frequency [4] and gas-phase temperature field [4, 5]. With so many measurements characterizing the 30 cm methanol pool fire, it is a suitable candidate for fire modeling validation studies [3, 6-8]. On the other hand, research on the detailed structure and dynamics of larger pool fires is limited. Tieszen, *et. al.* [9, 10] used particle imaging velocimetry to measure the mean velocity field in a series of 1 MW to 3 MW methane and hydrogen pool fires burning in a 1 m diameter burner. Klassen and Gore [11] reported on flame height and the heat flux distribution near 1.0 m diameter pool fires burning a number of fuels including methanol. They used the same burner as this study, but with a 5 mm (rather than 10 mm as used here) lip height. This study complements Ref. [11] by also measuring the local flame temperature throughout the flow field, the heat release rate using oxygen consumption calorimetry, and the radiative fraction determined by a single location measurement.

Use of fire modeling in fire protection engineering has increased dramatically during the last decade due to the development of practical computational fluid dynamics fire models and the decreased cost of computational power. Today, fire protection engineers use models like the Consolidated Fire and Smoke Transport Model (CFAST) and the Fire Dynamics Simulator (FDS) to design safer buildings, power plants, aircraft, trains, and marine vessels to name just a few types of applications [6, 12]. To be reliable, the models require validation, which involves a large collection of experimental measurements. An objective of this report is to provide data for use in fire model evaluation by the fire research community. Also, it is of interest to compare the burning characteristics of the 30 cm methanol pool fire with the results presented here for a 1 m diameter methanol pool fire.

2. Experimental Methods

Steady-state burning conditions were established before measurements were initiated. A warm-up period of 10 min was required for the mass burning rate to be steady. Since back diffusion of water slowly accumulates in the fuel pool in methanol fires, fresh fuel was used between experiments. The purity of the methanol was 99.99 % by mass and the density was 792.7 kg/m^3 at 20 °C, according to a report of analysis provided by the supplier. Experiments were conducted under an exhaust hood located 4 m above the burner rim. The effect of ambient convective currents on the fire were minimized by closing all inlet vents in the laboratory. The exhaust consisted of a large round duct (1.5 m diameter) located 6.0 m above the floor [13]. The smallest exhaust flow possible (about 4 kg/s) was used, helping to avoid perturbations (such as flame lean) and minimizing the influence of the exhaust on fire behavior. This led to the establishment of an unusually symmetric and recurring fire. The experiments were repeated three times.[*]

[*] Certain commercial entities, equipment, or materials may be identified in this document in order to describe an experimental procedure or concept adequately. Such identification is not intended to imply recommendation or endorsement by the National Institute of Standards and Technology, nor is it intended to imply that the entities, materials, or equipment are necessarily the best available for the purpose.

2.1. Pool Burner Setup

A circular steel pan with an inner diameter (*D*) of 1.00 m, a depth of 0.15 m, and a wall thickness of 0.0016 m held the liquid methanol. An image of the burner is seen in Fig. 1. The bottom of the burner was water cooled. The burner was mounted on cinder blocks such that the burner rim was about 0.3 m above the floor. A fuel overflow basin included for safety extended 3 cm beyond the burner wall at its base. The fuel inlet was insulated and covered with a reflective foil to prevent preheating of the fuel.

Fig. 1. The 1 m diameter, water-cooled, round steel burner with fuel level indicator and fuel overflow section. The S type thermocouple used to measure the gas phase temperature is also shown.

2.2. Measuring Heat flux

The radiative heat flux by the fire emitted to the surroundings was measured using a wide view angle, water-cooled, Gardon type total heat flux gauges with a 1.3 cm diameter face. The gauges were positioned as shown in Fig. 2. Radial heat flux gauges oriented upward were aligned with the burner rim to measure the heat flux towards the floor. Vertical heat flux gauges were used to measure heat flux to the surroundings.

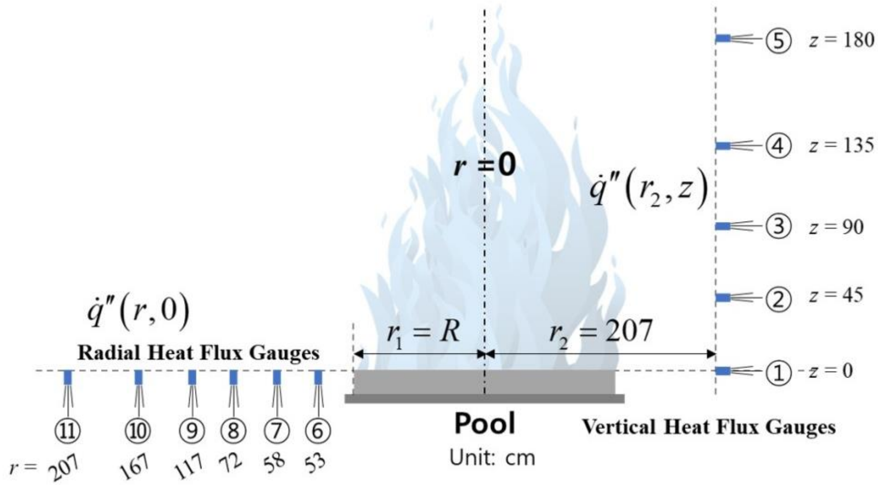

Fig. 2. A schematic diagram of the heat flux gauge set-up. All units in the figure are in cm.

2.3. Measuring Temperature

The local temperature was measured using a Type S (Pt, 10 % Rh/Pt), bare-wire, fine diameter thermocouple. The thermocouple was inserted into a (2-hole) 3 mm outer diameter ceramic tube with about 1 cm of the thermocouple wire including its bead, extending beyond the end of the ceramic tube. Selection of the diameter of a fine wire thermocouple must consider trade-offs between the durability of the instrument and measurement needs. The finer the wire, the smaller the radiative exchange with the environment and the faster the measurement time response, but the more difficult it is to configure. In this study, a 50 µm diameter S-type thermocouple was employed with an approximately spherical bead as observed using an optical microscope. The measured signal was acquired at a rate of 60 Hz for 120 s using a data acquisition module (SCXI-1600, National Instruments Inc.), which represents about 170 flame puffing cycles.

A computer-controlled translation device was used to adjust the position of the thermocouple along a vertical axis aligned with the pool centerline. The vertical rail was aligned with the centerline of the burner and the thermocouple/ceramic tube assembly was attached to the tip of a horizontal rod connected to the moving rail. The connection region between the thermocouple and the rod was well-insulated and covered with aluminum foil.

The energy balance on the thermocouple bead considers convective, radiative, and conductive heat transfer, and can be expressed as:

$$\dot{Q}_{conv} + \dot{Q}_{rad} = \rho_b \cdot c_{p,b} \cdot V_b \frac{dT_b}{dt} \quad (1)$$

where $\dot{Q}$ is the net rate of heat transfer. ρ, $c_{p,b}$, and V_b are the density, specific heat and volume of the bead, respectively. In addition, if the response time of the thermocouple is much larger than the fire fluctuation frequency, then thermal inertia effects can impact the measurement variance, although there is little influence on the mean [4]. The thermal inertia is related to the thermocouple time constant (τ), and the energy balance becomes:

$$T_g(t) = T_b(t) + \tau \frac{dT_b(t)}{dt} + \frac{\varepsilon\sigma}{h}\left(T_b^{\,4}(t) - T_{surr}^4\right) \tag{2}$$

$$\tau = \frac{m_b c_{p,b}}{hA_b} \tag{3}$$

where T_b is the bead temperature, T_g is the gas temperature, T_{surr} is the effective temperature of the surroundings, A_b is the surface area of the bead, σ is the Stefan-Boltzmann constant ($5.67 \cdot 10^{-8}$ W/m^2/K^4), ε is the thermocouple emissivity. Here, the flame is taken as essentially optically thin based on estimates using the radiation subroutine in Ref. [6]. The convective heat transfer coefficient of gas flow near the bead is defined as $h = \mathrm{Nu} \cdot \lambda_g / d_b$, where λ_g is the thermal conductivity of gas, d_b is the thermocouple bead diameter. In Eq. (2), the second and third terms on the right side represent the thermal inertia correction and radiation correction, respectively. The Nusselt number is empirically associated with the Reynolds and Prandtl numbers. Solving the thermal inertia correction term, the time derivative of bead temperature was calculated using a second-order polynomial fit of three consecutive data points of the temperature time series with a curve fit window size of 33.3 ms.

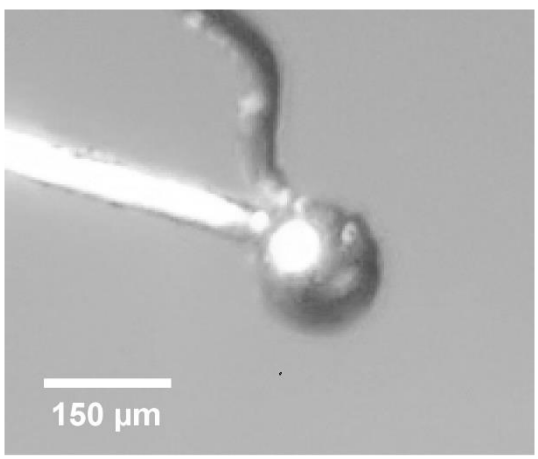

Fig. 3. Magnified image of thermocouple bead.

Fig. 3 shows an image of the thermocouple bead, which was approximately spherical with an eccentricity of about 0.97. The bead diameter was measured using Image-J image processing software from a photo taken with an optical microscope. The uncertainty of the bead diameter was multiplied by the image resolution (2.7 µm/pixel) and the number of pixels needed to determine the edge of the bead. The measured bead diameter was 153.3 µm ± 7.7 µm, which was approximately three times the wire diameter. The time constant for heat transfer to a sphere [14] can be written as:

$$\tau = \frac{\rho_b c_{p,b} {d_b}^2}{6 \mathrm{Nu} \lambda_g} \tag{4}$$

Following Shaddix [15], the Nusselt number for a sphere is calculated using the Ranz-Marshall model:

$$\mathrm{Nu} = 2.0 + 0.6\ \mathrm{Re}^{1/2}\ \mathrm{Pr}^{1/3}; \qquad 0 < \mathrm{Re} < 200 \tag{5}$$

where Re is the Reynolds number of the bead and Pr is the Prandtl number. The temperature-dependent gas properties for Re and Pr, are taken as those of air [16], and the temperature-dependent emissivity and thermophysical properties of platinum are taken from Refs. [15, 17]. The average ambient temperature during the experiments was 298 K ± 5 K, which was taken as the surrounding temperature, T_{surr}, in Eq. (2). A FDS simulation of the fire was conducted to validate the temperature correction method used to solve Eq. (2) and to obtain the gas velocity distribution above the burner to better represent Re in Eq. (5). The FDS input code was based on the FDS Validation Guide's [6] input file for the 1 m methanol pool fire case. Details are explained in Ref. [18]. The average difference in the mean gas temperature along the centerline between FDS and the experimental results was 4 %. FDS yielded Re ranging from 1 to 24 along the centerline. In Eq. (2), the radiation correction and thermal inertia correction terms mainly affect the mean and variance values, respectively, in agreement with Refs. [4, 15]. For example, correction of the mean temperature due to radiative loss along the centerline was 1 % on average, varying from near zero at the top of the fire plume to 1.7 % at the hottest fire locations. The thermal inertia correction term has a negligible influence on the mean gas temperature, but does amplify the value of its instantaneous extremes, which affects the local standard deviation. The average contribution of the thermal inertia correction term for locations along the centerline represents 54 % of the standard deviation of the gas temperature. In contrast, the radiative loss term has little influence. For these reasons, the uncertainties of the mean and standard deviation of the gas temperature were separately analyzed. The uncertainties of each term of the gas temperature in Eq. (2) were determined based on Ref. [19]. The calibration error of a Type S thermocouple is 0.25 % in $273\ \mathrm{K} < T_b < 1733\ \mathrm{K}$ [20]. The measurement uncertainty of the data acquisition (DAQ) system was approximately 0.60 % for the application range of the thermocouple [21].

3. Results and Discussion

The shape of the fire dramatically changed during its pulsing cycle. The fire was blue with no indication of the presence of soot. Fig. 4 shows four images of the methanol pool fire during different phases of its puffing cycle. Repeating puffing cycles occurred in which orderly curved flame sheets anchored at the burner rim were connected to the central fire plume, rolled towards the fire centerline, and necked-in to form a narrow and long visible fire plume. The flame height was recorded with 30 Hz video. Analysis of the video record showed that the average flame height and its standard deviation was 1.10 m ± 0.22 m and the primary pulsation frequency was 1.37 Hz ± 0.03 Hz.

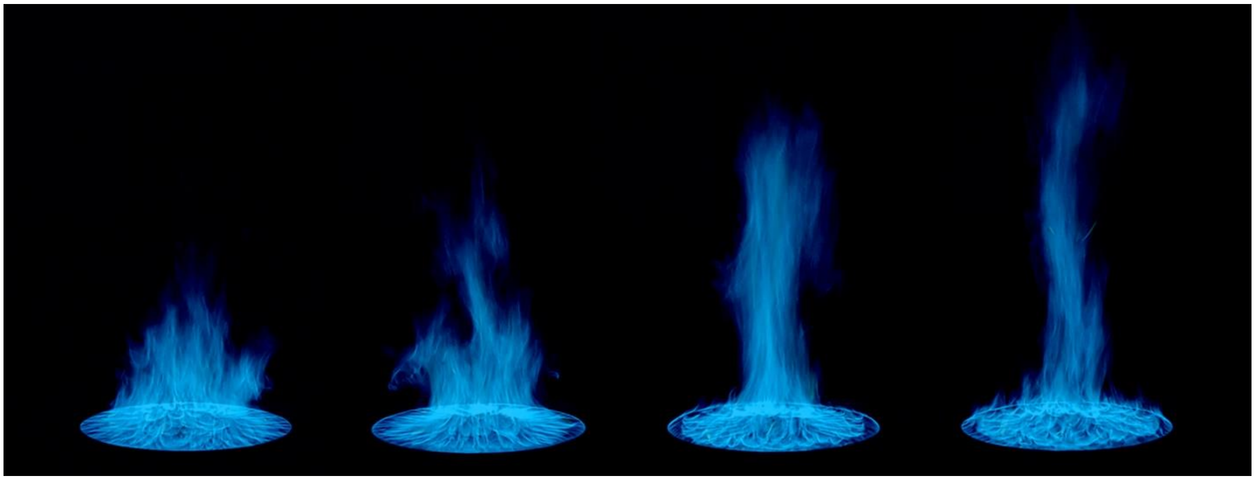

Fig. 4. Instantaneous digital images 132 ms apart in the pulsing 1 m diameter methanol pool fire.

3.1. Mass Burning Rate

With a steady liquid level in the fuel pool, the mass burning rate was measured by monitoring the mass loss in the 20 L methanol reservoir feeding the liquid pool, using a calibrated load cell. Fig. 5 shows the time-varying fuel mass in the reservoir during Test 3. When the fuel was low in the reservoir, it needed to be replenished. The periods when the reservoir was refilled are indicated by the white (unshaded) regions in Fig. 5. During these periods, the fuel was still fed to the burning pool and the fuel level in the pool was maintained constant as verified by a video camera focused on the relative level of the fuel compared to the fuel level indicator (see Fig 1). The burning rate is estimated during the gray regions in the figure, that is, after an initial warm-up and avoiding periods when fuel was added to the reservoir. The total mass loss rate for each period is noted (by the numbers in the gray regions) by considering the ratio of the mass loss to the duration of the period. The time-weighted mean mass burning rate during the three tests was 12.8 g/s ± 0.9 g/s, where the uncertainty here is reported as the combined expanded uncertainty, representing a 95 % confidence interval (a coverage factor of two).

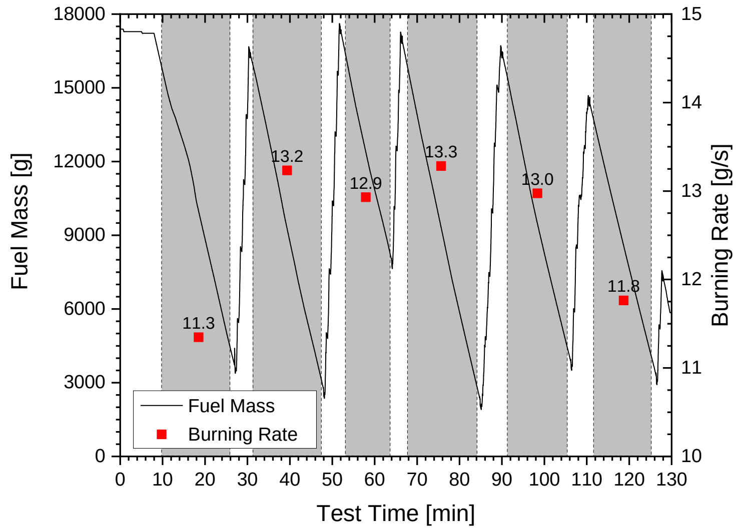

Fig. 5. Mass of fuel reservoir and average fuel burning rate during Test 3. The unshaded regions after 10 min represent times when the reservoir was being refilled with methanol.

3.2. Heat Release Rate

The heat release rate was measured using oxygen consumption calorimetry and compared with the ideal heat release rate ($\dot{Q}$) calculated from the mass burning rate, i.e., $\dot{m}\Delta H_c$, where ΔH_c is the net heat of combustion of methanol equal to 19.9 kJ/g [16]. The heat release rate from calorimetry was averaged for the three tests once the fire reached steady-state burning.

The measured mass burning rate, the ideal heat release rate, and heat release rate measured via the oxygen consumption calorimetry are presented in Table 1. As expected, the ideal heat release rate agrees well with the measured calorimetric heat release rate since the combustion efficiency is expected to be nearly 1. The heat release rate measured by calorimetry was 256 kW ± 45 kW, where the combined expanded uncertainty was based on repeat measurements, the results described in Ref. [13], and additional natural gas calibrations (at a measured heat release rate of about 250 kW).

Table 1. Measured mass burning rate in the 1 m methanol pool fire, the ideal heat release rate determined from the measured mass burning rate, and the heat release rate determined using calorimetry. The uncertainty is expressed as the combined expanded uncertainty with a coverage factor of two, representing a 95 % confidence interval.

Mass burning rate $\dot{m}$ [g/s]	Ideal Heat Release Rate $\dot{Q}$ [kW]	Heat Release Rate from calorimetry $\dot{Q}_a$ [kW]
12.8 ± 0.9	254 ± 19	256 ± 45

3.3. Heat Flux Distribution

Fig. 6 shows the mean radial radiative heat flux as a function of the radial distance from the burner centerline. As expected, the radiative heat flux rapidly decreases with distance from the centerline. The maximum measured radial heat flux was 5.1 kW/m^2 ± 1.0 kW/m^2. The heat flux consistently decreased in a manner proportional to $1/r^2$. Fig. 7 shows the mean vertical radiative heat flux as a function of the axial distance above the burner. There was little change in radiative heat flux in the axial direction. The radial heat flux has a maximum value of 1.0 kW/m^2 ± 0.1 kW/m^2 at 0.9 m above the burner. Fig. 6 also shows the results from Ref. [11], which are in agreement with the current measurements within experimental uncertainty.

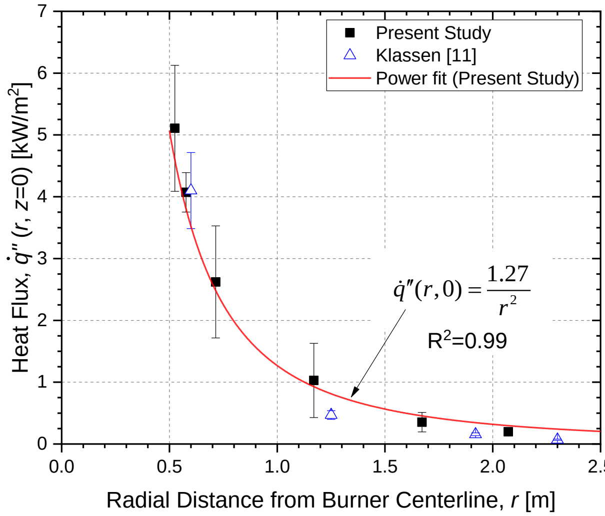

Fig. 6. Mean and standard deviation of the radial radiative heat flux as a function of the radial distance from the burner centerline at the plane defined by the burner rim (z = 0).

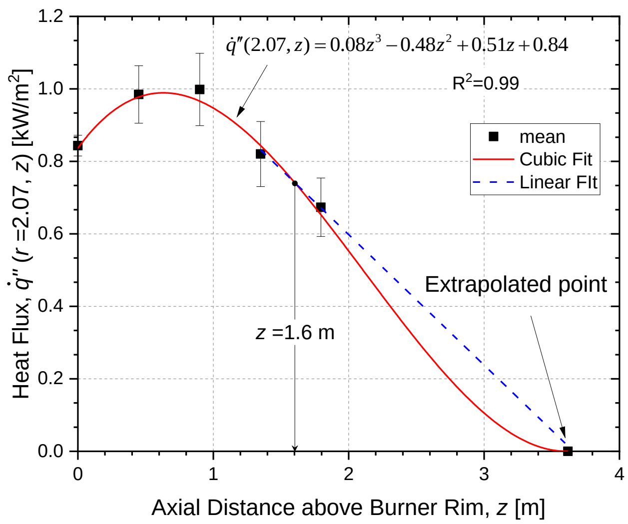

Fig. 7. Mean and standard deviation of the vertical radiative heat flux as a function of the axial distance above the burner for gauges facing the pool fire.

The fraction of energy radiated from the fire (χ_{rad}) was calculated as shown in Eqs. (6) and (7) , considering the overall enthalpy balance explained in Ref. [22], where its value is equal to the ratio of the total radiative emission from the fire $\dot{Q}_{rad}$ normalized by the idealized fire heat release rate ($\dot{Q}$). The radiative fraction can be broken into the sum of the radiative heat transfer to the surroundings (χ_r) and onto the fuel surface (χ_{sr}) such that:

$$\chi_{rad} = \chi_r + \chi_{sr} = \dot{Q}_{rad}/\dot{Q} \tag{6}$$

$$\chi_r = \dot{Q}_r/\dot{Q} \quad \text{and} \quad \chi_{sr} = \dot{Q}_{sr}/\dot{Q} \tag{7}$$

where $\dot{Q}_r$ is the radiative energy emitted by the fire to the surroundings except to the fuel surface and $\dot{Q}_{sr}$ is the radiative heat feedback to the fuel surface. Assuming symmetry, integrating the measured local radiative heat flux in the *r* and *z* directions (see Fig. 2) yields the total energy radiated by the fire, $\dot{Q}_{rad}$, considering the flux through a cylindrical control surface about the pool fire:

$$\dot{Q}_{rad} = \dot{Q}_r + \dot{Q}_{sr} = \left(2\pi\int_{r_1}^{r_2} \dot{q}''(r,0)\cdot r dr + 2\pi r_2 \int_0^{z_2} \dot{q}''(r_2,z)dz\right) + \pi r_1^2 \bar{\dot{q}}_{sr}'' \tag{8}$$

where r_1 and r_2 are 0.5 m and 2.07 m, z_2 is 3.62 m, and $\bar{\dot{q}}_{sr}''$ is the average radiative heat flux incident on the fuel surface. In the energy balance for a steadily burning pool fire following Ref. [22], the total heat feedback ($\dot{Q}_s$) to the fuel surface is broken into radiative and convective components ($\dot{Q}_s = \dot{Q}_{sr} + \dot{Q}_{sc}$). Normalizing this by $\dot{Q}$, $\chi_s = \chi_{sr} + \chi_{sc}$. Kim *et al.* [22] measured the distribution of local heat flux incident on the fuel surface in a 30 cm methanol pool fire. The fractional total heat feedback (χ_s) was 0.082 ± 24 % with about 67 % attributed to radiation, that is, χ_{sr}= 0.055 ± 21 %. χ_s in the 1 m pool fire is assumed to be the same as in the 30 cm pool fire. Convective heat transfer to the fuel surface ($\dot{Q}_{sc}$) was calculated using the thin film theory following [23]. As a result, χ_{sr} was 0.065 ± 31 % and χ_{sr}/χ_s was 0.80, which is about 20 % larger compared than in 30 cm pool fire. The fitting function seen in Figs. 6 and 7 was used to integrate the heat flux in the radial and vertical directions. The zero-heat flux position (z_2 = 3.62 m) was extrapolated from the values of the highest two locations in Fig. 7. In previous studies [11, 22], the heat flux peaked at a vertical position equal to approximately one-half the characteristic flame height and decreased almost linearly above the visible flame tip regardless of pool diameter and fuel type, until it reached zero. The vertical radiative heat flux (the second term in Eq. (8)) was integrated using the cubic function from 0 to z_1 (1.6 m) and either the cubic function or a line in the region from z_1 to z_2. The energy difference associated with the fitting functions was treated as uncertainty.

The results show that $\dot{Q}_{rad}$ was 56 kW ± 11 % and χ_{rad} was 0.22 ± 16 %. The radiative fraction of the total heat release rate emitted to the surroundings in previous studies for methanol pool fires is listed in Table 2. The radiative fraction reported here agrees with the value in Ref. [11] within expanded uncertainty. The radiative fraction of the 1 m pool fire was similar to its value in the 30 cm fire, and agreed with the result in Ref. [22] which suggested that the radiative fraction was fairly constant as a function of pool size for diameters less than 2 m.

Table 2. Comparison of the radiative fraction in steadily burning 30 cm and 100 cm methanol pool fires. The combined expanded uncertainty is also shown, representing a 95 % confidence interval.

Research	Pool diameter	χ_{rad}
Present study	100 cm	0.22 ± 16 %
Klassen and Gore [11]	100 cm	0.19[a,b]
Kim *et al.* [22]	30 cm	0.24 ± 25 %
Hamins *et al.* [24]	30 cm	0.22 ± 10 %

[a] $\bar{\dot{q}}_{sr}''$ in Eq. (8) was assumed equal to the heat flux measured next to the burner ($\dot{q}''$(51 cm, 0) = 4.1 kW/m^2), which yields χ_{sr} = 0.01, which is smaller than expected [22]. χ_{rad}, therefore, was recalculated with χ_{sr} = 0.055, yielding χ_{rad} = 0.19.

[b] Recalculated χ_{rad}, using ΔH_c = 19.918 kJ/g [16], not 22.37 kJ/g, assuming gaseous water as a product of combustion.

3.4. Temperature Distribution

Fig. 8 shows the measured time series of uncorrected bead temperature (T_b), the radiation corrected temperature (T_r) considering only the radiation correction term (not the thermal inertia) in Eq. (2), and the (radiation and inertia) corrected gas temperature (T_g). There is no time-delay between the bead temperature and the radiation corrected temperature. The radiative correction became larger as the bead temperature increased with the maximum correction equal to 55 K, when T_b =1694 K. The minimum correction was 7 K, when T_b =1070 K in Fig. 8. The corrected gas temperature was 617 K lower than the bead temperature at 40.35 s, whereas it was 313 K higher than the bead temperature at 40.68 s. The mean time constant was calculated as 57 ms ± 3 ms. As the Nusselt number increases with bead temperature, the time constant decreases, as indicated by Eq. (4).

Fig. 9 shows the measured mean and standard deviation of the bead temperature, corrected gas temperature and time constant as a function of distance above the burner along the centerline of the fire in Test 3. As expected, the mean gas temperatures were very similar to the mean bead temperature for all positions. On average, the combined expanded uncertainty of the mean gas temperature was 8 %, considering all 46 temperature measurement locations. On average, the combined expanded uncertainty of the standard deviation of gas temperature as 26 %.

The mean and standard deviation of the gas temperature as a function of distance above the burner along the centerline are shown in Fig. 10. The maximum value of the mean temperature was about 1371 K, which occurred at 0.3 m above the burner rim. The gradient near the fuel surface in Fig. 10 is steep. At 0.05 m above the burner, the gas temperature was about 1144 K ± 424 K. The temperature at two locations on the fuel surface was measured to be at the boiling point of methanol, 338 K, yielding a temperature gradient near the fuel surface of about 161 K/cm ± 85 K/cm.

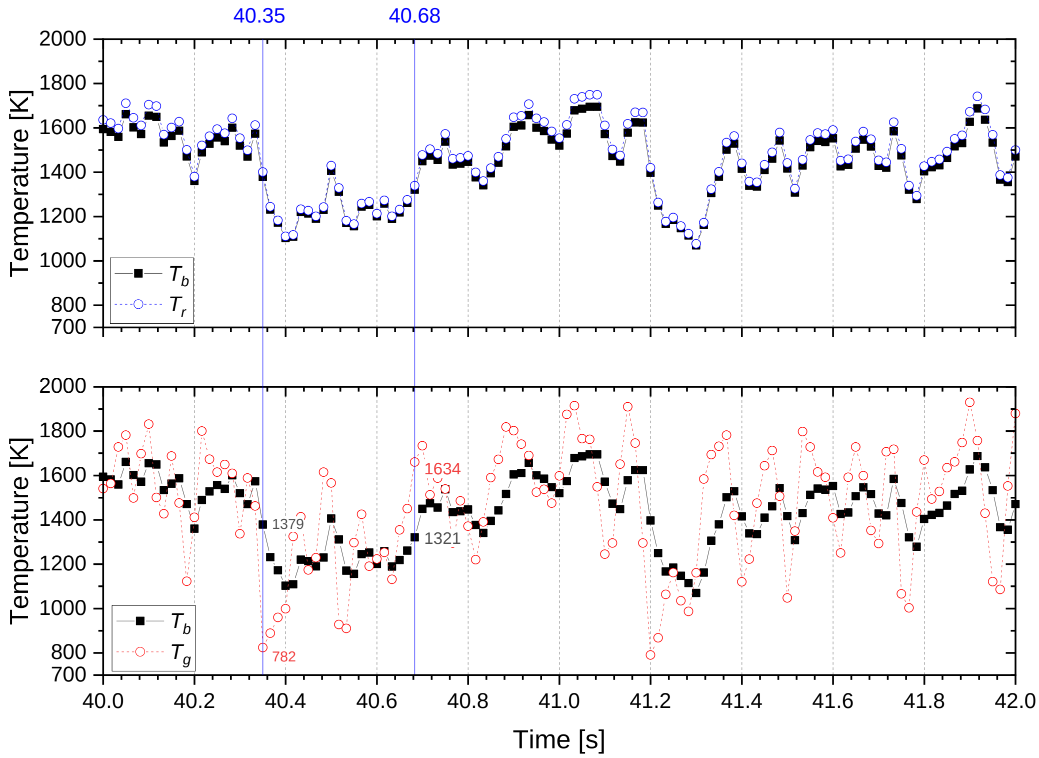

Fig. 8. Instantaneous temperature at (z, r) = (30 cm, 0 cm) in Test 3; T_b is the bead temperature, T_r is the corrected temperature considering only radiative loss, and T_g is the gas temperature corrected for radiative loss and thermal inertia.

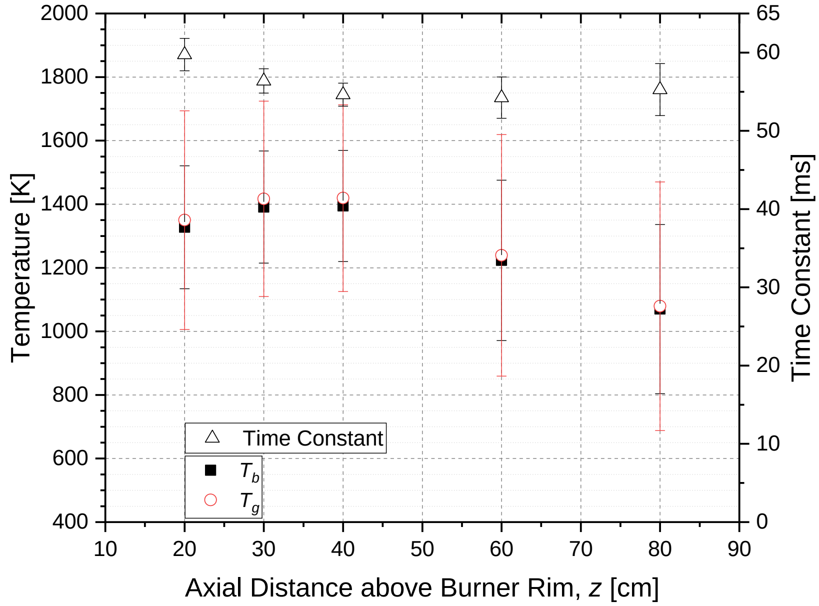

Fig. 9. Mean and standard deviation of the measured bead temperature profile, and calculated gas temperature and thermocouple time constant as a function of axial distance above the burner rim in Test 3.

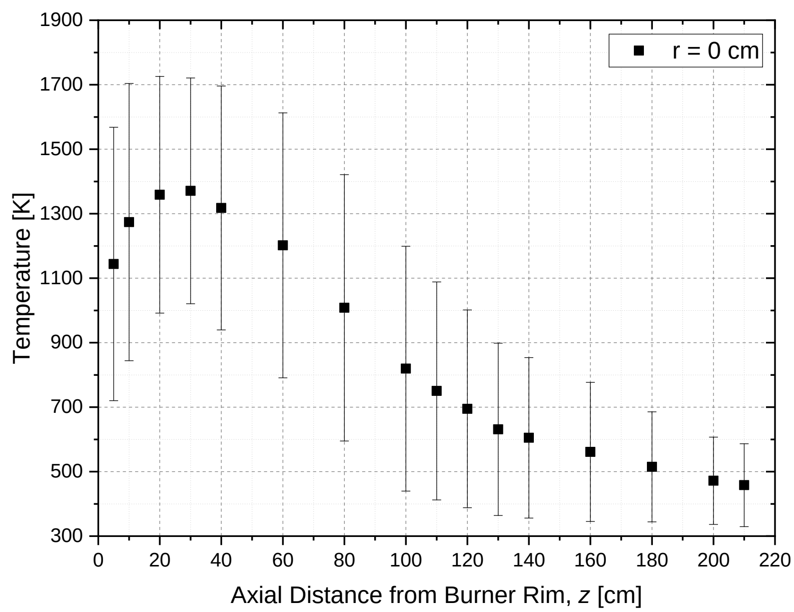

Fig. 10. Mean and standard deviation of the gas temperature profile as a function of axial distance above the burner rim along the centerline of the fire.

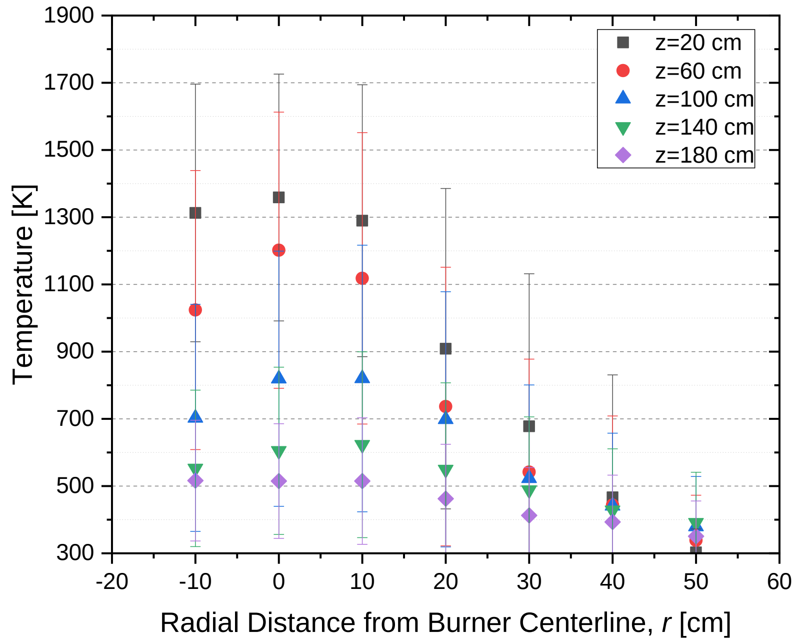

Fig. 11. Mean and standard deviation of the gas temperature profiles as a function of radial distance from the burner centerline at various heights above the burner rim.

Fig. 11 shows the mean and standard deviation of the gas temperature profile in the radial direction for various axial distances above the burner rim (20 cm $\leq z \leq$ 180 cm). The maximum temperature occurs near the centerline for each elevation. The gradient diminished with distance from the fuel surface. A complete discussion of the uncertainty analysis for the temperature and other results is given in Ref. [18].

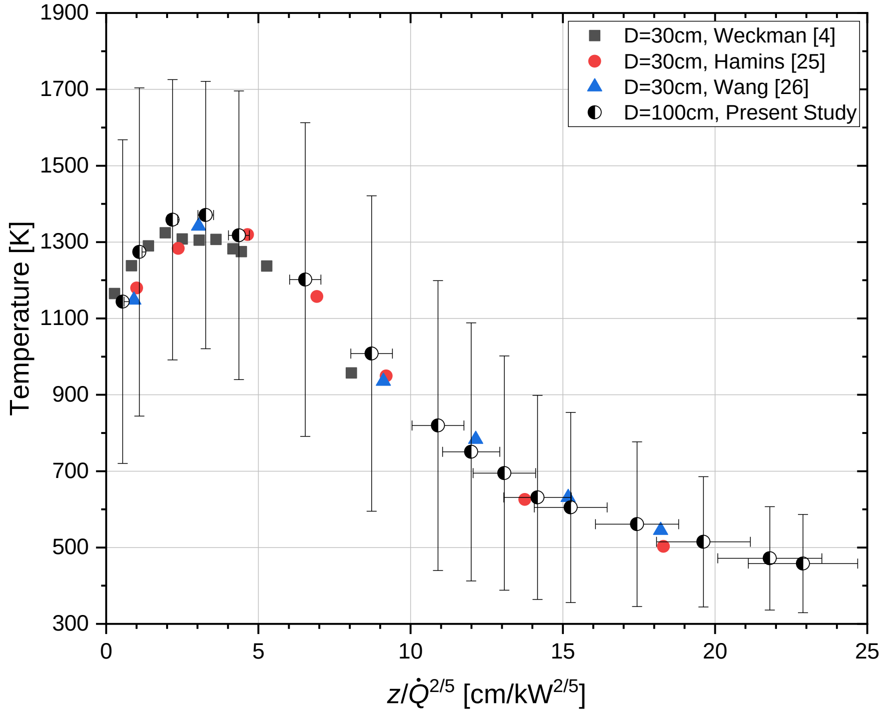

Fig. 12. Mean and standard deviation of the axial temperature profiles as a function of distance above the burner rim normalized by $\dot{Q}^{2/5}$ and compared to previous results in 30 cm methanol pool fires.

Fig. 12 shows the mean and standard deviation of the temperature profile as a function of scaled axial distance. The results are compared to previous measurements in 30 cm diameter methanol pool fires from Refs. [4, 25, 26]. Axial distance above the burner is normalized by $\dot{Q}^{2/5}$ following Baum and McCaffrey [27]. Weckman and Strong [4] measured temperature in a 30.5 cm diameter methanol pool fire with a lip height of 1 cm using a 50 µm wire diameter, bare bead, Type S (Pt, 10% Rh/Pt), thermocouple similar to the thermocouples used in this study. The measurements from Ref. [25] are also shown, where temperature was measured using a 75 µm wire diameter, bare bead, Type S thermocouple in a steadily burning 30.1 cm diameter methanol pool fire with a 0.6 cm lip. The radiation corrected thermocouple measurements in Wang *et al.* [26] are also shown, using a 50 µm wire diameter, bare bead, Type S thermocouple in a steadily burning 30.1 cm diameter methanol pool fire with a 1 cm lip height. A comparison of the results in Fig. 12 shows that the 1 m and 30 cm pool temperatures are similar when the axial distance above the burner is normalized by $\dot{Q}^{2/5}$.

4. Summary and Conclusions

A series of measurements for temperature, burning rate and heat release rate were conducted to characterize a 1 m diameter, well-ventilated methanol pool fire steadily burning in a quiescent environment. The measured heat release rate determined by oxygen consumption calorimetry was 256 kW ± 45 kW, which was consistent with the heat release rate calculated from the fuel mass burning rate measurements. The gas-phase thermocouple temperature measurements were corrected considering radiative loss and thermal inertia effects. Instantaneous temperatures as large as 1800 K were measured in the fire. The maximum value of the time-averaged gas temperature was measured as about 1371 K, which occurred about 0.3 m above the burner. As expected, the corrected profile of mean axial temperature was shown to be similar to previous results for methanol pool fires when scaled by $\dot{Q}^{2/5}$. The heat flux was measured in the radial and vertical directions, and the radiative fraction was estimated as 0.22 ± 16 %, which corresponded to previous methanol pool fire results in 1 m and 0.3 m diameter pools. The present results help provide an understanding of the structure and character of the 1 m diameter methanol pool fire and provide data useful for the evaluation of fire models.

Acknowledgements

The authors are grateful to Marco Fernandez of NIST for assistance with the measurements.

References

[1] K Akita, T Yumoto, Heat transfer in small pools and rates of burning of liquid methanol, Proceedings of the Combustion Institute 10 (1965) 943-948.

[2] A Hamins, S J Fischer, T Kashiwagi, M E Klassen, J P Gore, Heat feedback to the fuel surface in pool fires, Combustion Science and Technology 97 (1994) 37-62.

[3] S Hostikka, K B Mcgrattan, A Hamins, Numerical modeling of pool fires using LES and finite volume method for radiation, Fire Safety Science 7 (2003) 383-394.

[4] E J Weckman, A B Strong, Experimental investigation of the turbulence structure of medium-scale methanol pool fires, Combustion and Flame 105 (1996) 245-266.

[5] A Yilmaz, Radiation transport measurements in methanol pool fires with Fourier transform infrared spectroscopy, NIST Grant/Contractor Report GCR 09-922, January 2009.

[6] K McGrattan, R McDermott, M Vanella, S Hostikka, J Floyd, C Weinschenk, K Overholt, Fire dynamics simulator user's guide, NIST special publication 1019, National Institute of Standards and Technology, October 2019.

[7] G Maragkos, T Beji, B Merci, Towards predictive simulations of gaseous pool fires, Proceedings of the Combustion Institute 37 (2019) 3927-3934.

[8] Z Chen, J Wen, B Xu, S Dembele, Large eddy simulation of a medium-scale methanol pool fire using the extended eddy dissipation concept, International Journal of Heat and Mass Transfer 70 (2014) 389-408.

[9] S R Tieszen, T J O'Hern, R W Schefer, E J Weckman, T K Blanchat, Experimental study of the flow field in and around a one meter diameter methane fire, Combustion and Flame 129 (2002) 378-391.

[10] S R Tieszen, T J O'Hern, E J Weckman, R W Schefer, Experimental study of the effect of fuel mass flux on a 1-m-diameter methane fire and comparison with a hydrogen fire, Combustion and Flame 139 (2004) 126-141.

[11] M Klassen, J Gore, Structure and radiation properties of pool fires, NIST-GCR-94-651, National Institute of Standards and Technology, Gaithersburg, MD, June 1994.

[12] R D Peacock, W Jones, P Reneke, G Forney, CFAST–consolidated model of fire growth and smoke transport (version 6) user's guide, NIST special publication 1041r1 (2013)

[13] R A Bryant, M F Bundy, The NIST 20 MW calorimetry measurement system for large-fire research, NIST Technical Note 2077, National Institute of Standards and Technology, Gaithersburg, MD, 2019.

[14] T L Bergman, F P Incropera, D P DeWitt, A S Lavine, Fundamentals of heat and mass transfer, John Wiley & Sons, 2011.

[15] C R Shaddix, Correcting thermocouple measurements for radiation loss: A critical review, American Society of Mechanical Engineers, New York, Sandia National Labs., Livermore, CA (US), 1999.

[16] Design institute for physical properties (DIPPR 801), American Institute of Chemical Engineers, 2017.

[17] F M Jaeger, E Rosenbohm, The exact formulae for the true and mean specific heats of platinum between 0 ° and 1600 ℃, Physica 6 (1939) 1123-1125.

[18] K Sung, J Chen, M Bundy, M Fernandez, A Hamins, The thermal character of a 1 m methanol pool fire, NIST Technical Note 2083, National Institute of Standards and Technology, Gaithersburg, MD, 2020.

[19] B N Taylor, C E Kuyatt, Guidelines for evaluating and expressing the uncertainty of NIST measurement results, NIST Technical Note 1297, National Institute of Standards and Technology, Gaithersburg, MD, 1994.

[20] The temperature handbook, Omega Engineering Inc., 2004, pp. Z-39-40.

[21] SCXI-1600 user manual and specifications, National Instruments Inc., 2004.

[22] S C Kim, K Y Lee, A Hamins, Energy balance in medium-scale methanol, ethanol, and acetone pool fires, Fire Safety Journal 107 (2019) 44-53.

[23] L Orloff, J de Ris, Froude modeling of pool fires, Technical Report FMRC OHON3.BU, RC81-BT-9, Factory Mutual Research Corp., Norwood, MA, 1983.

[24] A Hamins, M Klassen, J Gore, T Kashiwagi, Estimate of flame radiance via a single location measurement in liquid pool fires, Combustion and Flame 86 (1991) 223-228.

[25] A Hamins, A Lock, The structure of a moderate-scale methanol pool fire, NIST Technical Note 1928, National Institute of Standards and Technology, Gaithersburg, MD, 2016.

[26] Z Wang, W C Tam, K Y Lee, A Hamins, Temperature field measurements using thin filament pyrometry in a medium-scale methanol pool fire, NIST Technical Note 2031, National Institute of Standards and Technology, Gaithersburg, MD, 2018.

[27] H R Baum, B McCaffrey, Fire induced flow field-theory and experiment, Fire Safety Science 2 (1989) 129-148.